Fossil Fuels

Comparative Study of the Effect of Fuel Deoxygenation and Polar Species Removal on Jet Fuel Surface Deposition

Ehsan Alborzi, Phil Gadsby, M. S. Ismail, Abdolkarim Sheikhansari, Matthew Dwyer, Anthony J. H. M. Meijer, Simon Blakey, and Mohamed Pourkashanian

Just Accepted

Comparative Study of the Effect of Fuel Deoxygenation and Polar Species Removal on Jet Fuel Surface Deposition

Ehsan Alborzi,[*,†] Phil Gadsby,[†] Mohammed S. Ismail,[†] Abdolkarim Sheikhansari,[†] Matthew. R. Dwyer,[†] Anthony J. H. M. Meijer,[‡] Simon G. Blakey,[¶] and Mohamed Pourkashanian[†]

[†]*Department of Mechanical Engineering, The University of Sheffield, Sheffield S3 7HF, UK*

[‡]*Department of Chemistry, The University of Sheffield, Sheffield, Sheffield S3 7HF, UK*

[¶]*Department of Mechanical Engineering, The University of Birmingham, Birmingham B15 2TT, UK*

E-mail: e.alborzi@sheffield.ac.uk

Abstract

The effect of near-complete deoxygenation and polar species removal on deposition propensity of a Jet A-1 fuel type, with marginal thermal oxidative stability was studied in a laboratory scale approach. The fuel deoxygenation was carried out via nitrogen purging and two types of bespoke zeolites were used separately in a packed bed reactor for partial polar separation. The treated fuel samples were assessed individually for deposition propensity, using "High Reynolds Thermal Stability(HiReTS)" test device. It was found that when the concentration of hydroperoxides in fuel is relatively high, polar removal is more effective way than the fuel deoxygenation in reducing carbonaceous deposits.

Furthermore, competitive adsorption of dissolved O_2 with polar species was studied for a model fuel doped with a few polar species, as well as for the Jet A-1 with marginal thermal stability, in the packed bed reactor with zeolite 3.7Å. The polar species added to the model fuel share the same functional groups as those in Jet A-1 with a strong impact on fuel thermal degradation and surface deposition. These include hexanoic acids, heaxnol, hexanal, hexanone, phenyl amine (aniline), butylated hydroxytoluene(BHT), dibutyl disulfide and Fe naphthenate.

A one-dimensional model for calculation of dissolved O_2 adsorption in the packed bed reactor was built using COMSOL Multiphysics. The modelling results were in good agreement with the induction period prior to the beginning of the O_2 adsorption, as well as the different stages of O_2 uptake during the competitive adsorption between dissolved O_2 and polar species in the Jet A-1 fuel. The calculation showed a discrepancy with the experimental results beyond the second phase of O_2 adsorption. More theories, assumptions and physical sub-models are required to build a more robust predictive model.

A new chemical reaction pathway based on the self-reaction of hydroperoxides was proposed as part of "Basic Autoxidation Scheme(BAS)" to justify the relatively high deposition propensity of the marginal fuel after near-complete deoxygenation. The viability of this reaction pathway was supported by the quantum chemistry calculations.

Introduction

## Overview of chemistry of fuel autoxidation

Gas turbine fuels are exposed to thermal stress en-route from the fuel tank, through the engine fuel supply system to the combustion chamber. The increasing temperature of fuel, as it passes through the engine fuel supply system, initiates a multitude of chemical reactions in bulk fuel.[1] This results in the formation of a number of soluble and insoluble complex

organic molecules which are composed of hydrocarbons, sulfur, nitrogen and oxygen.[2] These

species ultimately contribute to the formation of carbonaceous deposits on the surface of the

fuel system. These deposits can block filter screens or fuel nozzles, cause disruption to the

flow of fuel, and result in breakdown in the operation of specific engine components.

Different chemical pathways contribute to the changes in chemical composition of a ther-

mally stressed jet fuel. Each of these needs a temperature at which they will dominate the

formation of deposits. Using analytical grade n-dodecane as a simplified model fuel, Reddy[3]

reported three temperature regimes. These include the autoxidation dominant, which oc-

curs at the temperatures up to $300\,°C$, and the pyrolytic degradation, which proceeds at the

temperature regimes above $500\,°C$. There is also an intermediate region reported that falls

between the autoxidation and pyrolytic regimes.

Aviation fuel typically contains approximately $70\,ppm$ of dissolved O_2, when is in equilibrium

with air at atmospheric pressure and at room temperature. The molecular O_2 initiates a

multitude of chemical reactions known as autoxidation. The autoxidation of liquid hydro-

carbons has been broadly studied for pure single component hydrocarbons, with the carbon

atom numbers in the range of petroleum based jet fuel (C_{10}-C_{12}). The results of these stud-

ies indicate that the autoxidation reactions proceed through a free radical mechanism.[4–7]

The initiation step of autoxidation is manifested by the formation of free alkyl radicals, as

presented schematically in rxn1. It is hypothesised that the catalytic effect of metal con-

stituents of the fuel wetted surface plays a significant role in the initiation of autoxidation.[5]

Through the propagation stage, the free radicals can react with dissolved oxygen as shown

in rxn2. Another typical reaction in the propagation stage, which is rate determining, is the

abstraction of one hydrogen atom from the substrate by $RO_2\,\cdot$, generating a hydroperoxide

and an alkyl radical in conformity with the rxn3.

$$RH \longrightarrow R\cdot \tag{1}$$

$$R\cdot + O_2 \longrightarrow RO_2\cdot \tag{2}$$

$$RO_2\cdot + RH \longrightarrow RO_2H + R\cdot \tag{3}$$
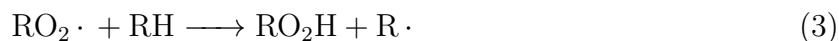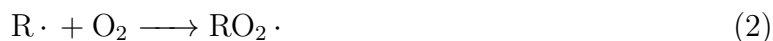
64 There is much experimental evidence indicating that trace polar species including phenolic

65 species[8,9] , reactive sulfur species such as sulfides and disulfides[10,11] and nitrogen compo-

66 nents[12–16] play a significant role in the overall rate of autoxidation and surface deposition.

67 The intervention of antioxidants is through the H-atom abstraction reaction from peroxy

68 radicals as illustrated in rxn4. This reaction proceeds faster than the rxn3 due to the lower

69 activation energy. Therefore, jet fuels with high concentration of phenolic compounds tend

70 to oxidise slowly. However, these species have a significant impact on the increase of depo-

71 sition rate.[17]

72

73 Hydroperoxides are another influential class of chemical species which significantly affect the

74 overall rate of autoxidation.[1] It is important to note that hydroperoxides are inevitably found

75 in micro-molar concentration in Jet-A1 during the storage period.[18] This class of species is

76 also considered as the primary products of fuel autoxidation. However, they are suscep-

77 tible to be thermally and/or catalytically decomposed under thermal exposure, as shown

78 schematically in rxn5. Thermal decomposition of hydroperoxides is integrated into the "Ba-

79 sic Autoxidation Scheme(BAS)" of liquid hydrocarbon fuels to account for the maintenance

80 of propagation stage in the absence of dissolved oxygen.[19,20]

81

82 As shown in rxn5, hydroperoxides partly undergo thermal decomposition(homolitic fission).

83 However, reactions catalysed by the intervention of complexes of dissolved metals such as

84 Cu, Fe and Mn cause this class of reaction proceed with a faster rate.[18,21] It is known that

85 due to the low polarity of hydrocarbons, metals are not directly soluble in aviation fuels.

86 However, the trace of metals are identified in aviation fuel in association with naturally oc-

87 curring organic ligands. It is hypothesised that the organic ligand species are most likely to

88 be a mixture of naphthenic acids. Fuel contacts different metal components during produc-

89 tion and supply chains, which results in binding with naphthenic acids in the fuel, forming

90 fuel soluble metal naphthenates.[22]

91

Another chemical pathway for decomposition of hydroperoxides is through the non-radical

reactions with reactive sulfurs as illustrated in rxn6 and rxn7.[11] It is reported that reactive

sulfurs and products of phenolic species in association with indoles and/or carbazoles con-

tribute to the surface deposition.[4,18] However the underlying theory of the physico-chemical

interactions of these species is not well understood. With the exception of nitrogen com-

pounds, the role of the most significant heteroatomic species in fuel autoxidative deposition

process is illustrated schematically in figure 1.

$$AH + RO_2\cdot \longrightarrow RO_2H + A\cdot \qquad (4)$$

$$ROOH \longrightarrow RO\cdot + \cdot OH \qquad (5)$$

$$ROOH + RSR \longrightarrow ROH + \text{sulfoxide} \qquad (6)$$

$$\text{ROOH} + \text{RSSR} \longrightarrow \text{ROH} + \text{thiosulfinate} \tag{7}$$
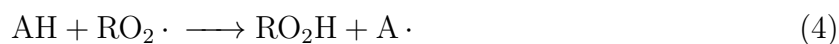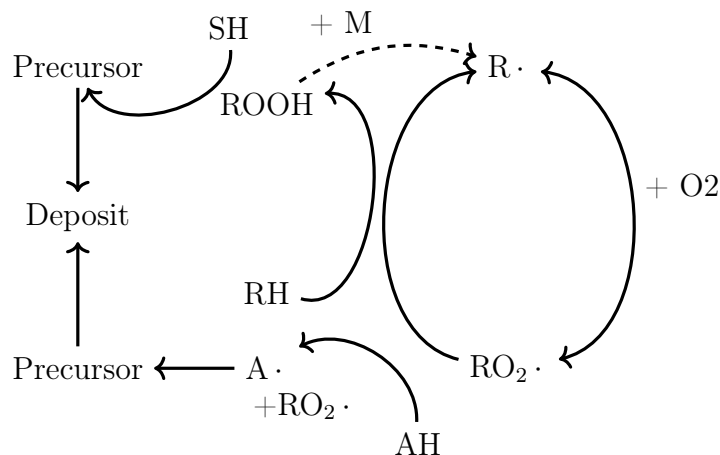
Figure 1: Autoxidation Scheme for liquid hydrocarbons along with pathways leading to deposit formation, adapted from[18]

Fuel cleansing through partial adsorptive separation of polar species and dissolved oxygen

Deoxygenation of aviation fuel via nitrogen purging has been widely used as a laboratory scale method for jet fuel thermal oxidative stability enhancement. In theory, this is achieved by prevention of peroxy radicals formation in rxn2. Membrane separation[23] is another method for aviation fuel deoxygenation by which a significant O_2 drop from 70 ppm to less than 1 ppm is reported. There is much experiential evidence to suggest that the positive impact of deoxygenation on surface deposition could be significantly different. This depends on the distribution of trace sulfur, nitrogen containing molecules and oxygenated species in the fuel.[10,12,24,25]

Attapulgus clay is widely used at refineries as part of wet treating processes and also is com-

104 monly utilised in places close to the airports in the US, to remove surface active components

105 and other polar species. This is of great importance considering that aviation fuel is trans-

106 ported through multi-product supply chains and it may pick up trace of polars from previous

107 delivery and distribution of other fuels.[26,27] Zeolite is another type of solid adsorbent used

108 for aviation fuel deoxygenation with low efficacy in the lab scale applications.[28]

109

110 It is known that zeolites are highly porous crystalline aluminosilicates. Numerous zeo-

111 lite species (with different chemical compositions, crystal structure and adsorption proper-

112 ties) are known. In general, zeolites are described as aluminosilicates with open 3-dimensional

113 framework structures. They include corner-sharing TO_4 tetrahedra, where T is Si^{4+} and Al^{3+}

114 which are loosely associated with framework oxygens O^{2-}. Each oxygen anion connects two

115 cations and this yields a macro-molecular three dimensional framework with neutral SiO_2

116 and negatively charged AlO_2^- tetrahedral building-blocks. The negative charge is compen-

117 sated by additional non-framework cations such as Na^+ which is generally present after the

118 synthesis of the zeolite. The crystalline structure of zeolite is honeycombed with relatively

119 large cavities. Each cavity is connected through apertures or pores. The exact diameter of

120 the pore depends on the coordination, type and the amount of cations and anions.[29,30]

121

122 Due to the presence of alumina, zeolites exhibit a negatively charged framework which is

123 counter-balanced by positive cations. This results in a strong electrostatic field on the

124 internal surface. Cations can be exchanged to calibrate the pore size or the adsorption

125 characteristics. In theory, the ability to fine-tune the pores to determined uniform openings

126 allows molecules smaller than the pore diameter to diffuse in whilst excluding the larger

127 molecules, known as the confinement effect.[29] The molecular size discrimination by zeolites

128 for branched hydrocarbons in comparison to the linear hydrocarbon molecules is reported in

129 the literature.[31]

130

131 In addition to the selective adsorption by pore size, larger molecules can be adsorbed on the

132 surface of pores of zeolites as a result of three major interactions: Van der Waals forces be-

133 tween zeolite pore walls and the adsorbate; electrostatic interactions between the adsorbate

134 and Brönsted acid sites of zeolite; and the adsorbate-adsorbate interactions.[32] For instance,

135 adsorption of alcohols in zeolites occurs through hydrogen bonding between the OH func-

136 tional group with zeolite Brönsted acid sites. Furthermore, it is shown that with addition

137 of carbon atom, the dispersion forces, which are the result of the interactions between the

138 adsorbate and zeolite pore walls, become crucial factor in the adsorption affinity of the al-

139 cohols.[33]

140

141 In summary, the net effect of interactions between guest molecules and zeolites is controlled

142 by the ratio of Si/Al.[34] Therefore, it is expected to observe a variety of chemisorption and

143 physisorption of polar and non-polar species into the pores and surfaces of zeolites. For

144 instance, studies using "Density Functional Theory(DFT)" demonstrated that zeolites ex-

145 hibit both physisorption and chemisorption in binding with molecules such as CO_2, CO and

146 H_2.[35–37] It is also reported that zeolites with smaller pore size show preferential adsorption

147 between H_2, CH_4 and N_2 based on the molecular size. In contrast, it is shown that O_2 will

148 bind with Al with the possibility of chemical interaction.[38] This is an important consid-

149 eration when investigating the binding of autoxidation products with zeolites as not only

150 structure and size will be dominant factors but the chemical composition of zeolites can play

151 an important role.

152

153 One of the advantages of zeolites in the adsorption process is the sorbent regenerating char-

154 acteristics. There are common methods for regeneration of zeolites which can be grouped

155 into four types, used separately or in combination.[30] These include thermal swing, pressure

156 swing, purge gas stripping and displacement cycle.

157

158 This study aims to compare the impact of near-complete fuel deoxygenation with partial po-

159 lar species removal on propensity of surface carbonaceous deposits. This work is laboratory-

160 scale; scaling-up for larger applications and higher level of technology readiness requires

161 serious engineering considerations and was not part of this study.

162

Experimental Work

Baseline fuels and chemical composition

165 Three baseline fuels were used in this study: two types of Jet A-1 and a model fuel (i.e. a

166 polar-free solvent composed of 5 normal paraffins in the range of C_{10} to C_{14}). The compo-

167 sition of major hydrocarbon constituents and the most significant deposition related to the

168 polar species of the baseline fuels are shown in table1.

169

170 The Jet A-1 fuel samples were analysed for hydrocarbons, reactive sulfurs and antioxidants

171 externally, using a test method developed by Intertek UK. This method identifies sulfur con-

172 taining compounds and group types in the middle distillates using an Agilent 7890 N "Gas

173 Chromatograph(GC)" equipped with a Zoex thermal modulation and an Agilent 355 sulfur

174 chemiluminescence detector. Fuel acidity was also quantified by Intertek UK according to

175 the ASTM D3242.

176

177 Quantification of sulfur classes was carried out via normalisation to the total sulfur content

178 as determined by combustion followed by UV-Fluorescence. The $GC \times GC$ analysis separates

179 sulfur-containing compounds based on their boiling points and polarity. Thus it was possi-

180 ble to elute the benzothiophenes and dibenzothiophenes in two well-defined bands, clearly

181 separated from the band of thiophenes, sulfides and mercaptans. Hydrocarbon speciation

182 was carried out using "UOP Method 990-11". This method determines the molecular type

183 homologous series based on the carbon number.

184

185 The polar nitrogen was quantified externally by "University of Dayton Research Institute

186 (UDRI)", using multidimensional gas chromatography time of flight mass spectrometry, fol-

187 lowing the analytical method reported in the reference.[15] Dissolved metal analysis was per-

188 formed in our lab using a calibrated Spectro-Ciros-Vision ICP-OES instrument. The total

189 concentration of hydroperoxide in the baseline fuels were determined in our lab following the

190 test method reported in the reference.[20]

191

Table 1: Composition of major hydrocarbon constituents along with sulfur, polar nitrogen, hydroperoxides and dissolved metals for the baseline fuels

	Baseline Fuel		
	Fuel sample A	Fuel sample B	Polar-free solvent
Chemical composition	**Concentration**		
n-Paraffins	20.67% m/m	19.56% m/m	97.2% m/m
iso-Paraffins	24.77% m/m	25.83% m/m	NA
cyclics	30.84% m/m	31.92% m/m	NA
Alkylbenzenes	16.18% m/m	15.12% m/m	1.1 %
Indans and tetralins	2.15% m/m	2.1% m/m	NA
Naphtalenes	1.33% m/m	1.28% m/m	NA
Antioxidant	25 mg/l	25 mg/l	NA
Acidity	0.08 $mgKOH/100g$	0.072 $mgKOH/100g$	NA
Thiols, Sulfides and Disulfides	835 mg/kg	812 mg/Kg	NA
Polar Nitrogen	12 mg/kg	12 mg/kg	NA
Total hydroperoxides	13.8 μM	4.1 μM	2.5 μM
Dissolved Fe	115 ppb	110 ppb	NA
Dissolved Cu	50 ppb	38 ppb	NA
Dissolved Zn	48 ppb	64 ppb	NA

Fuel thermal oxidative stability assessment

193 A HiReTS test device was used to assess the thermal stability of the baseline fuels and

194 treated fuels for comparison. This test device is based on the ASTM D6811-02 test method.

195 In this method, an aerated test fuel is filtered and pumped through an electrically heated

196 capillary at turbulent regime. The capillary tube is controlled to maintain a constant fuel

197 temperature of 290 °C at the tube exit.

198

199 The external surface of capillary is blackened to give a high thermal emissivity such that a

200 pyrometer can measure the real-time changes in the capillary wall temperature with the high

201 degree of accuracy. Over time, the deposition of the carbonaceous materials on the inner

202 surface of capillary tube causes an insulative effect. This results in localised areas of elevated

203 external wall temperature. Our previous findings show that the profile of temperature rise

204 along a heated tube in aero-engine representative condition is non-linear and fuel specific.

205 The non-linear temperature rise along the external surface of a simulated burner feed arm

206 under engine representative condition is reported in references.[39,40]

207

208 By virtue of mounting a pyrometer on an automated positioning bed, the temperature in

209 the localised areas can be captured as discrete measurement points, along a small section

210 of the capillary, and used to create a time-profile of temperature rise along the wall. The

211 main advantage of the HiReTS method is the ability to quantify the thermal stability of fuel

212 using relative measures such as HiReTS number. This number corresponds to the thickness

213 of deposit inferred from the change to the thermal conduction between fuel and wetted wall.

214 The calculation of the HiReTS number employs the difference between the final and minimum

215 ΔT measurement in the data set generated at each of the twelve measurement positions. The

216 total HiReTS number is calculated by summing this difference at each measurement position

217 as shown in equation1. The test condition used in HiReTS is presented in table2.

Table 2: Test conditions in HiReTS

Test Parameters	Values
Flow Rate(ml/min)	35
Test temperature(°C)	290
Test Pressure(MPa)	2.0
Test Time(min)	120
Number of positions measured per scan(n)	12
Scans per test	25
Distance between measured position(mm)	2.5
Fuel aeration time(min)	12
Scan time(min)	5

$$\sum_{n=1}^{n=12} (\Delta T_{Final} - \Delta T_{min}) \tag{1}$$

Fuel deoxygenation and adsorptive fuel treatment

The effect of near-complete deoxygenation on deposition propensity of the baseline fuels was carried out using N_2 purging. Prior to the N_2 purging, the baseline fuels were aerated, as indicated in the ASTM D6811-02 test method. Level of fuel deoxygenation was monitored by an optical oxygen sensor which operates based on fluorescence quenching technology. The deoxygenated fuel samples were kept in sealed fuel drums to minimise the risk of ambient air diffusion and were instantly assessed for the surface deposition propensity in the HiReTS test device.

A packed bed reactor was used to explore the simultaneous effect of zeolites 3.7Å and 4.5Å on partial fuel deoxygenation and polar species removal. The packed bed reactor was a 1 m stainless steel tube with a 2.54 cm inner diameter and 6 K-type thermocouples inserted equally distant along the tube for temperature monitoring. The distance between two neighbouring thermocouples was 15 cm.

A "Proportional Integral Derivative (PID)"controller was used to heat the furnace up to a fixed set point temperature for each test. Once the furnace reached the set point temperature and settled, the tube reactor was filled up with sorbent and fuel and subsequently placed inside the furnace. If the tube was connected to the pump prior to the furnace warming up, the time required to fill the tube would have been longer. In this situation, adsorption capacity of solid adsorbent could have been changed due to the longer interaction with the fuel. Due to the absence of cooling effect, once the furnace reached the set point temperature, the time required for fuel inside the tube to reach to the set point is faster in comparison to the flowing system. This helps to reduce the effect of gradual temperature rise on the air solubility in fuel.[27]

The amount of zeolite was fixed in such away to fill up the isothermal region of the packed

245 bed reactor. Subsequently, a fixed low flow rate of 5 ml/min was set by means of a pump as

246 a part of solvent delivery system in a "High Performance Liquid Chromatography(HPLC)".

247 This was to create a long residence time for the adsorption process in the bed. The level

248 of dissolved O_2 was monitored in-line by the optical oxygen sensor during each test. The

249 position of the oxygen sensor was approximately 1 m downstream of the tube reactor. Since

250 a standard complete HiReTS test requires 5 L of jet fuel(including test volume and rinsing),

251 each test took approximately 17 h to obtain sufficient volume for thermal stability assess-

252 ment in the HiReTS. It is important to note that three separate tests were carried out to find

253 the temperature corresponding to the beginning of the adsorption. This was in the range

254 of 25 to 75°C for both zeolites. Since dissolved O_2 was monitored in-line, the beginning of

255 adsorption was based on O_2.

256
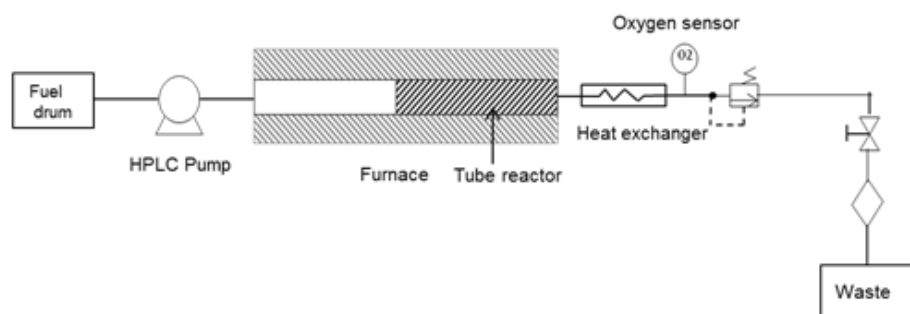
Figure 2: Schematic of packed bed reactor

257 To explore one by one interaction of the polar species with zeolites, the model fuel was doped

258 with the known amount of polar species individually. This was followed by the adsorptive

259 treatment using 10 ml cartridges, filled with 1 g sorbent. The cartridges were connected to

260 a vacuum manifold so that a fixed flow rate of 1 drop/s was set for the treatment. The list

261 of polar species and their concentrations in the model fuel is shown in table3. We deliber-

262 ately added higher concentrations to the model fuel to minimise the quantification errors.

263 It is worth to note that, although the selected polar species in this work share the same

264 functional groups in their molecular structures with the polar species in a typical Jet A-1,

265 their molecular weight is significantly lower. Concentration of polar species in the treated

266 samples were measured by gas chromatography with the exception of Fe naphthenate which

267 was quantified by ICP-OES.

268

269 To explore the competitive adsorption between dissolved O_2 and polar species with zeolite,

270 the model fuel doped with the polar species was treated with zeolite 3.7Å in the packed

271 bed reactor. The amount of dissolved O_2 in the treated fuel samples was measured in-line

272 by the optical oxygen sensor. The same measurement techniques as above were used for

273 quantification of polar species. In the next stage, the marginal fuel was treated with 3.7Å in

274 the packed bed reactor under the same test condition used for the model fuel for comparison.

275 The reason for the use of zeolite 3.7Å rather than 4.5Å in the packed bed reactor was merely

276 the availability of the raw materiel(chabazite) for the preparation of the coated pellets by

277 the sorbent producer.

278

Table 3: List of polar species and concentration in model fuel

Polar species	Supplier	Concentration
Hexanoic acid(analytical grade)	Sigma-Aldrich	200 ppm
Hexanol(analytical grade)	Sigma-Aldrich	200 ppm
Hexanal(analytical grade)	Sigma-Aldrich	200 ppm
Hexanone(analytical grade)	Sigma-Aldrich	200 ppm
Cumene hydroperoxides(analytical grade)	Sigma-Aldrich	200 ppm
Dibutyl disulfide(analytical grade)	Sigma-Aldrich	200 ppm
Phenylamine(aniline)(analytical grade)	Sigma-Aldrich	200 ppm
Butylated hydroxytoluene(BHT)(analytical grade)	Sigma-Aldrich	200 ppm
0.012-0.015 mM Fe naphthenate(12% wt)	Fisher Scientific	200 ppb

Numerical Work

Packed bed reactor modelling

281 Two main approaches for simulation of diffusion in zeolites can be used including microscopic

282 and macroscopic methods. In the microscopic approach, the kinetic properties of guest

283 molecules are explicitly considered in modelling. However, in the macroscopic approach,

284 the zeolite is viewed as a continuous medium and kinetic properties of guest molecules are

285 neglected. The macroscopic approach is advantageous as it can be used as a fast correlative

286 model; the microscopic model is computationally expensive as it incorporates a variety of as-

287 sumptions regarding individual particle motion, the interaction between the guest molecule

288 and its host and interaction between the molecules themselves. Due to the complexity of

289 jet fuel chemical composition, we used a macroscopic model assuming that the jet fuel is a

290 binary mixture of a substrate and dissolved O_2 with the concentration of 70 ppm.

291

292 We assumed that the change of kinetics of O_2 adsorption over time is an indication for

293 the competitive adsorption of other classes of species. Accordingly, a time-dependent, one

294 dimensional model was created to calculate the adsorptive behaviour of dissolved O_2 in jet

295 fuel via passing through a bed of zeolite 3.7Å. It was also assumed that the concentration of

296 O_2 present in the mixture is small compared to the bulk fluid. Taking this into consideration,

297 the transport of diluted species in porous media interface in COMSOL Multiphysics with

298 convection and adsorption sub models was used. The convective/diffusive equations used in

299 the interface is shown in the equation2.

$$\frac{\partial c_i}{\partial t} + \nabla.(-D.\nabla.c_i) + \mathbf{u}.\nabla.c_i = R_i \tag{2}$$

300 Where c_i represents the concentration of component i in mol/cm^3, D_i denotes the diffusion

301 coefficient in m^2/s and R_i represents an expression for reaction rate of species i in $mol/m^3.s$

302 and $\mathbf{u}$ indicates the bulk average velocity of the fluid phase in m/s.

303

304 The first term on the left side of the equation accounts for the consumption (or accumula-

305 tion) of the species i. The second term corresponds to the diffusive transport with respect to

306 the interaction between the dilute species and the solvent. The third term on the left hand

307 side of the equation illustrates the convective transport due to the average bulk velocity $\mathbf{u}$.

308 The reaction source term on the right-hand side of mass balance equation accounts for a

309 chemical reaction or desorption of species i on a porous matrix.

310

311 The diffusive transport is solved in conformity with the Fick's law and the effective diffusion

312 in porous medium was calculated according to the equation3. Freundlich model was used to

313 solve the the adsorption of O_2 into the porous media.

$$D_e = \frac{\epsilon_p}{\tau_F} D_L \qquad (3)$$

314 Where D_L represents the single phase diffusion coefficient for the species diluted in pure liq-

315 uid phase in m^2/s, and τ_F accounts for the turtosity factor(dimensionless) and ϵ_p represents

316 the porosity of medium. The transport of diluted species interface in COMSOL provides

317 predefined expressions to calculate the turtosity factor in porous media according to the

318 Millington and Quirk model.

319

320 The initial conditions and parameters used in the modelling are shown in table4.

Table 4: Initial conditions and parameters used in the modelling

Tube reactor inner diameter	0.0254 m
Tube reactor length	1 m
Packed bed length	0.5 m
Concentration of dissolved oxygen in jet fuel	1.8E-3 mol/l
Concentration of bulk fuel	4.7 mol/l
Fuel flow rate	5 ml/min
Zeolite porosity	0.47
Diffusion coefficient of molecular oxygen	5E-6m^2/s
Diffusion coefficient of bulk fuel	1E-7m^2/s
Freundlich constant for oxygen	1.8
Freundlich exponent for oxygen	6

321 The diffusion of molecules in a pore is classified in different regimes depending on the pore

322 diameter. Accordingly, for macro-pores, which are of the order of $1\,\mu$m or larger, collisions

323 between the adsorbing molecules occur much more frequently than collisions with the ad-

324 sorbent and the wall. As a result, molecular diffusion becomes the dominant mechanism.

325 The number of collisions of adsorbing molecules with the wall increases as the size of pores

326 decreases until it eventually becomes smaller than the mean free path of the molecules. At

327 this point, Knudsen adsorption dominates and the molecular motion begins to be a function

328 of pore size. For example, in the range of 20Å , when the pore diameter becomes compa-

329 rable to the size of the adsorbing molecules, the ongoing molecules-wall interactions occur.

330 Diffusion in the micro pores of zeolites usually occurs in this regime which is known as config-

331 urational diffusion. Under this regime of diffusion, the molecular motion is strongly affected

332 by the exact size and shape of the zeolites' channels, the shape of the diffusing molecules,

333 the interactions between the surface atoms and the diffusing molecules, temperature and

334 concentration of the adsorbing molecules. As a consequence, it is quite challenging to derive

335 generalised equations where all these aspects are included in diffusion coefficients for the

336 systems. The values of diffusion coefficients in this case vary in a broad range from 10^{-8} to

337 $10^{-20} \mathrm{m}^2 \mathrm{s}^{-1}$. The readers are referred to the reference[41] for further information.

338

Quantum chemistry

340 Density Functional Theory (DFT) geometry optimisation and frequency calculations were

341 carried out in the Gaussian 09 program at the UB3LYP/cc-pVTZ/IEF-PCM (Heptane) level

342 of theory.[42–48] All structures were calculated using the singlet wave functions with the HOMO

343 and LUMO mixed to break the symmetry of the system and allow them to be open shell

344 singlet species.

345

346 The geometries of reactants, products and transitions states of the peroxides reactions were

347 all calculated. The reactants and products were considered optimised if the frequency cal-

348 culation had no imaginary frequencies. The transition states were considered optimised if

349 they had a single imaginary frequency along the reaction coordinate of interest. The opti-

350 mised structure for all of the calculations can be found in the supporting information. The

351 Arrhenius parameters were obtained from the DFT calculations using the thermodynamic

352 parameters from the frequency calculations.[49]

353

354 From the equations below,[23] the Arrhenius equation can be linked to the enthalpy and en-

355 tropy of the reactions. The activation energy(Ea) was taken as the enthalpy change between

356 the reactants and the transition states, and pre-exponential factor(A) was obtained from the

357 entropic term.

358

359 The rate of a chemical reaction can be given from by the Arrhenius equation, where A is

360 pre-exponential collision factor and Ea is the activation energy as shown in equation4.

361

$$k = A \ exp(\frac{-Ea}{RT})$$ (4)

362 The rate constant can also be written as illustrated in 5, where the pre-exponential factor

363 has been split up into a temperature dependent component and an entropic component.

364

$$k = \frac{KbT}{h} exp(\frac{\Delta S}{R}) \ exp(\frac{-Ea}{RT})$$ (5)

365 In a solvent, the activation energy can be substituted for the enthalpy of activation as pre-

366 sented in equation6.

367

$$k = \frac{KbT}{h} exp(\frac{\Delta S}{R}) \ exp(\frac{-\Delta H}{RT})$$ (6)

368 This indicates that the Arrhenius pre-exponential factor can be calculated using equation7.

369

$$A = \frac{KbT}{h} exp(\frac{\Delta S}{R})$$ (7)

Results and Discussion

Effect of deoxygenation on surface deposition propensity of baseline fuels

Given surface deposition propensity of the baseline fuels, hereafter fuel sample A is referred to as marginal fuel and fuel sample B as stable fuel respectively. The impact of near-complete deoxygenation on deposition propensity of baseline fuels is shown in figure3a. This effect on marginal fuel results in a noticeable reduction in deposition propensity. Nevertheless, the high value of the HiReTS number demonstrates that deoxygenated marginal fuel is still highly thermally unstable.

It can be observed that the impact of near-completed deoxygenation on deposition propensity of stable fuel is positive; however, this fuel was already very thermally stable to show a significant enhancement in surface deposition tendency. The model fuel was highly thermally stable due to the absence of polar species. Due to the drastic response of marginal fuel to the change of surface deposition propensity with near-complete deoxygenation, this fuel was used for further investigation in this work.
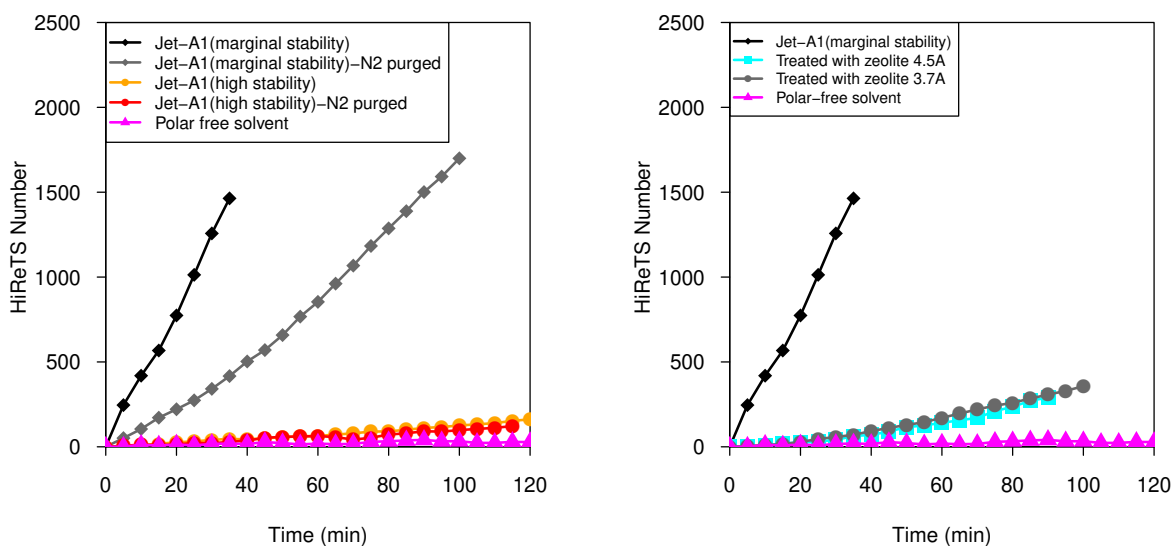
(a) Effect of near-complete deoxygenation on deposition

(b) Effect of polar species removal on deposition

Figure 3: a) Effect of near-complete deoxygenation via N_2 purging on deposition propensity of baseline fuels, b) Effect of polar species removal on deposition propensity of marginal fuel

In conformity with the kinetics of autoxidation in BAS[7] , in the presence of O_2 in bulk fuel, rxn2 requires no activation energy and it therefore proceeds very fast. Subsequently, $RO_2 \cdot$ reacts slowly with RH generating RO_2H and $R \cdot$. The literature data for the activation energy required for this reaction are in the range of 10-18 $kcal\,mol^{-1}$.[7,18] A related point to consider is that the generated $RO_2 \cdot$ can react with the radicals originating from phenolic antioxidant, as illustrated schematically in figure1. This reaction is one of the possible ways that leads to the formation of precursor molecules for the generation of surface deposits.

In theory, when fuel is deoxygenated, rxn2 cannot proceed; therefore the formation of $RO_2 \cdot$ via routine autoxidation pathways is interrupted. Hypothetically, this should disrupt the propagation stage and consequently the formation of deposit precursor, linked to the reaction of $RO_2 \cdot$, and radical of phenolic antioxidant is prevented. However, it was observed that, despite near-complete deoxygenation, marginal fuel exhibits a high deposition propensity. In

400 addition, despite substantial enhancement in surface deposition propensity of marginal fuel

401 via treatment with zeolites, the treated fuel showed an increasing deposition tendency over

402 time in the HiReTS test device.

403

404 To explain these behaviours, chemical analysis of the post-treated samples as well as the

405 results of individual interaction of the limited number of polar species with zeolites were

406 used as discussed below.

407

408 Comparison of one by one interaction of selected polar species with

409 zeolites

410 The results of one by one interaction of polar species with zeolites are presented in figure4.

411 The percentage of removal shown in the figure is defined in conformity with the equation 8.

$$\% \ removal = \frac{amount \ of \ polar \ in \ treated \ sample}{amount \ of \ polar \ in \ model \ fuel \ doped \ with \ polar \ prior \ to \ the \ treatment} \times 100 \quad (8)$$

412 It can be observed that the highest percentage of removal corresponds to the oxygenated

413 species with a decreasing trend from hexanoic acid to hexanal. The trend continues to de-

414 cline steadily from hexanal to aniline and BHT, followed by a substantial drop to dibutyl

415 disulfide. The overall trend of percentage of adsorption is the same for both zeolites; how-

416 ever, zeolite 4.7Å presents slightly higher adsorption. This is likely to be attributed to the

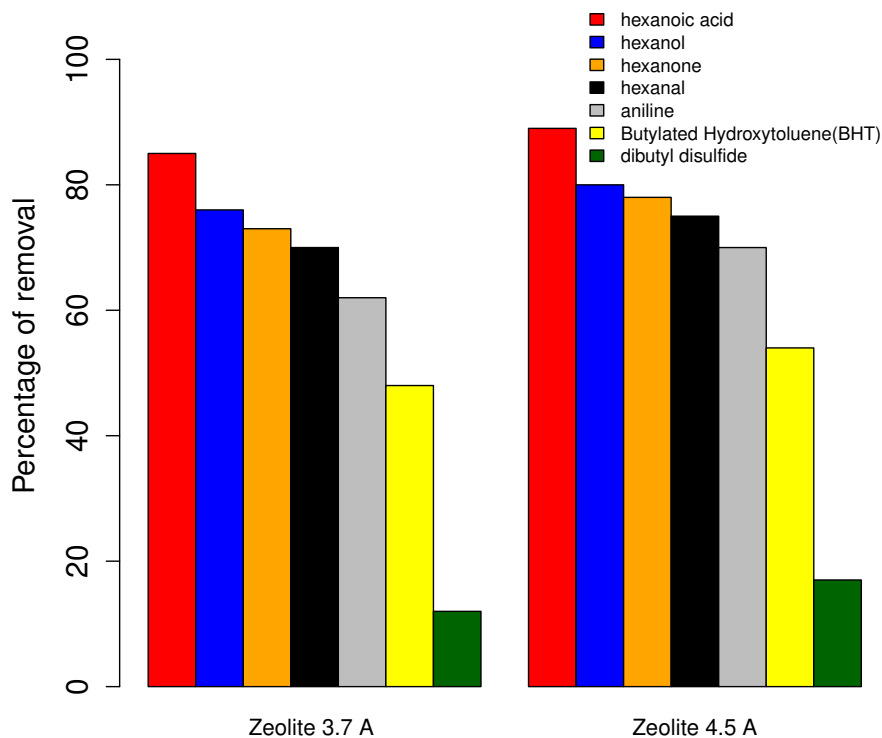417 bigger pore size, given that the ratio of Si/Al was the same for both zeolites.

418

Figure 4: One by one adsorption of polar species by zeolites 3.7Å and 4.5Å

The investigation of the intermolecular interactions of polar species in zeolites requires extensive molecular modelling work which is currently under way. Alternatively, we used "Hansen Solubility Parameter(HSP)"[50] as a simplistic approach to interpret the results presented in the figure4. HSP is defined in terms of three parameters for each molecule, including dispersion(δ_D), dipole moment(δ_P) and hydrogen bonding(δ_D), as shown in equation9.[50]

$$\delta^2 = \delta D^2 + \delta P^2 + \delta H^2 \qquad (9)$$

Table5 presents the estimated solubility parameters for the selected polar species, using HSPiP 5th Edition 5.1.04 software.[51] The HSP values were used to present three dimensional

427 vectors corresponding to the model fuel and the polar species in a spatial region known as

428 the Hansen space. Geometrical presentation of this space is not presented here due to the

429 complexity for the interpretation. Instead, the distance between two vectors in this space

430 can be used as the likelihood of intermolecular interactions between two species in such away

431 that the closer they are, the more solubility(interactions) they have. We calculated the dis-

432 tance of the polar species from the model fuel in conformity with the equation10; see figure5.

433

$$Ra^2 = 4(\delta D1 - \delta D2)^2 + (\delta P1 - \delta P2)^2 + (\delta H1 - \delta H2)^2 \tag{10}$$

434 The results shown in the figure5 indicate that the molecular interactions between the model

435 fuel and the oxygenated polars, as well as aniline, is relatively lower than BHT and dibutyl

436 disulfide . Given that the hydrogen bonding term for the oxygenated species and aniline is

437 higher, it is expected to observe that these species show the higher percentage of removal by

438 zeolites than BHT and dibutyl disulfide.

439

440 Contrary to the higher molecular interactions of BHT with the model fuel, the percentage

441 of removal of this species by zeolites indicates a high adsorption propensity. This is likely to

442 be attributed to the role of π-electrons of aromatic ring in forming hydrogen bonding with

443 the Brönsted acid sites of zeolite as reported in the reference.[52]

444

445 The lowest percentage of removal of dibutyl disulfide by zeolites is likely to be attributed to

446 the low electrostatic interactions of this species with the Brönsted acid sites of the zeolites.

447 In addition, the branched molecular structure of dibutyl disulfide might be a preventing

448 factor for diffusion through the pores. The results of adsorption of cumene hydroperoxide

449 and Fe naphthenate were not conclusive, hence are not presented in this article.

450

451 One of the limitations of HSP values is the uncertainties for the dipole moment parameter

452 and hydrogen bonding term for some species.[53] For instance, the estimated value of the hy-

453 drogen bonding term for hexanoic acid is incorrectly lower than heaxnol. It is important to

454 note that the $O-H$ group in carboxylic acids is more strongly polarised than the $O-H$ group

455 of alcohols due to the presence of the adjacent carbonyl group($C=O$). In fact, the dipole

456 present in carboxylic acids allows these spices to participate in hydrogen bonding, behaving

457 as both H-bond donor and acceptor. Such a high tendency of carboxylic acids for hydrogen

458 bonding is a strong justification for the highest percentage of removal of hexanoic acid when

459 compared to the other polar species.

460

Table 5: Hansen Solubility Parameters for the model fuel and polar species

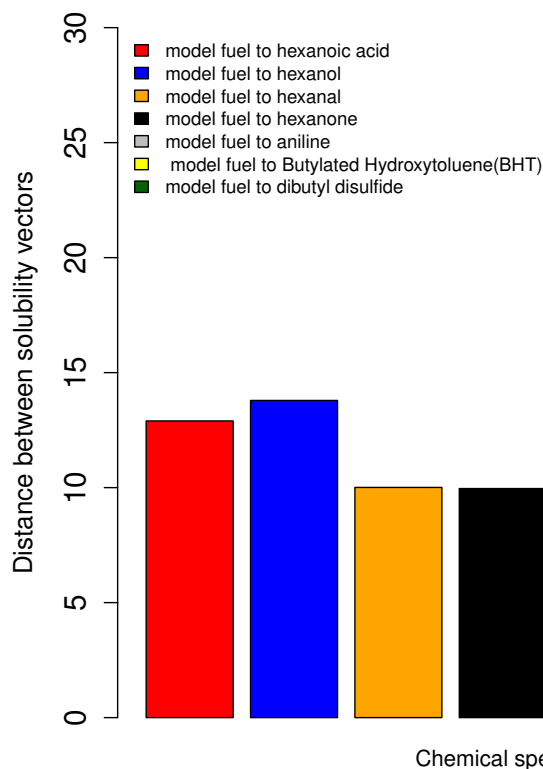| Chemical species	Hansen Solubility Parameters		
	Dispersion($MP^{0.5}$)	Dipole moment($MP^{0.5}$)	Hydrogen bonding($MP^{0.5}$)
Model fuel(n-dodecane)	16.2	0	0
Hexanoic acid	16.3	4.2	12.2
1-Hexanol	15.9	5.8	12.5
1-Hexanal	15.8	8.4	5.3
1-Hexanone	17.2	6.2	7.6
Aniline	19.4	5.1	10.2
BHT	16.5	0.9	4.5
Dibutyl disulfide	16.4	4.1	2.6

Figure 5: Distance between vectors of the model fuel and polar species

Investigation of competitive adsorption between O_2 and polars on zeolite 3.7Å in the packed bed reactor

The result of O_2 adsorption onto zeolite 3.7Å bed from model fuel doped with the polar species, carried out in the packed bed reactor, is shown in figure6a.

(a) Adsorption of O_2
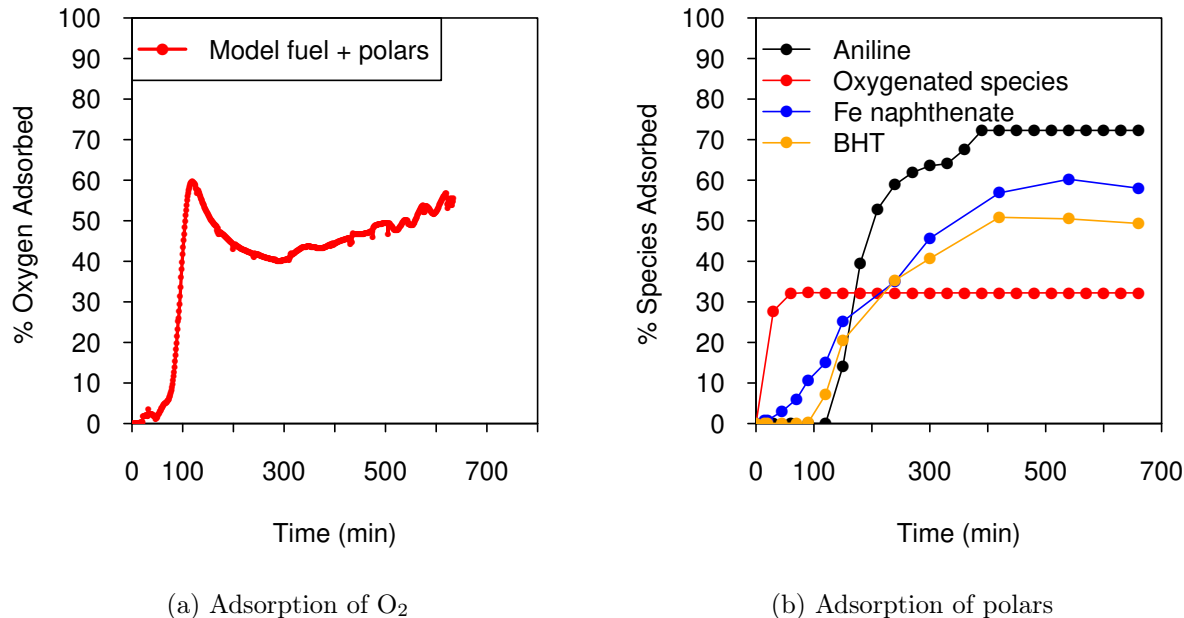
(b) Adsorption of polars

Figure 6: a) Multi stage adsorption of O_2 from model fuel doped with the polar species, b) Adsorption of polar species from model fuel doped with the polar species, the samples for polar separation were taken through a valve, 2 m downstream of the packed bed

465   The results indicate that the O_2 adsorption begins approximately after 60-70 min of the test.

466   This is followed by 60% increase over a period of 50-60 min, and an immediate decrease

467   for the next 120 min. The reduction of O_2 adsorption is relatively sharp at the beginning

468   and decelerates gradually for the next 180 min. A turning point, to which we refer as the

469   beginning of the second phase of O_2 adsorption, occurred at approximately 300 min of the

470   test time. During this phase, O_2 adsorption increased linearly.

471

472   The change in O_2 adsorption over time is likely to be attributed to a complex competitive

473   adsorption between polar species and dissolved O_2 as supported by the results shown in

474   figure6b. It can be observed that the oxygenated groups such as alcohol, aldehyde, ketone

475   and acids collectively adsorbed by the zeolite 3.7Å within the first 60 min of the experiment.

476   Fe naphthenate showed a slower adsorption rate in comparison to the oxygenated species.

477   However, the results indicate that uptake capacity of zeolite 3.7Å for Fe naphthenate is mod-

478 erately higher than the oxygenated species. It is likely that the first delay in O_2 adsorption

479 shown in figure6a is linked to the fast kinetics of the oxygenated species and Fe naphthenate

480 in zeolite 3.7Å.

481

482 Adsorption of BHT and aniline started at approximately same time (with BHT slightly

483 earlier). This time corresponds to the reduction of O_2 adsorption, as shown in figure6a.

484 The adsorption of BHT, Fe naphthenate and aniline reached a plateau after approximately

485 350 min of the test. This point matches with the beginning of the second phase of O_2 ad-

486 sorption. The results of adsorption of cumene hydroperoxide and dibutyl disulfide were not

487 conclusive and therefore were not presented here.

488

489 The results shown in the figure7a indicate that the adsorption of O_2 from marginal fuel,

490 followed the same trend as the model fuel doped with polar species with different timing. It

491 can be seen that O_2 adsorption started moderately after approximately 30 min but decreased

492 substantially over time. Subsequently, O_2 adsorption increased gradually in a linear trend

493 over the next 350 min. Such a long delay prior to the substantial O_2 adsorption is likely

494 to be attributed to the lower concentration of polar species in the marginal fuel. That is

495 to say, the time required for bed saturation for the case of model fuel doped with higher

496 concentration of polar species is shorter than the real fuel containing lower concentrations

497 of polar species.

498

499 A sudden increase in O_2 adsorption was observed after approximately 450 min with a max-

500 imum of 60% reached in about 50-60 min. The maximum level achieved is identical to the

501 case of the model fuel doped with the polar species. After this point, O_2 adsorption de-

502 creased with the same trend as the model fuel. However, a longer test for the marginal

503 fuel is required to observe if the second phase of O_2 can take place. The results of figure7b

504 indicate that the adsorption of Fe-bonded species and BHT from the marginal fuel followed

505 the same trend as model fuel doped with polar species; however, the time needed to reach

506 to plateau for these polars are different for marginal and model fuels.

507
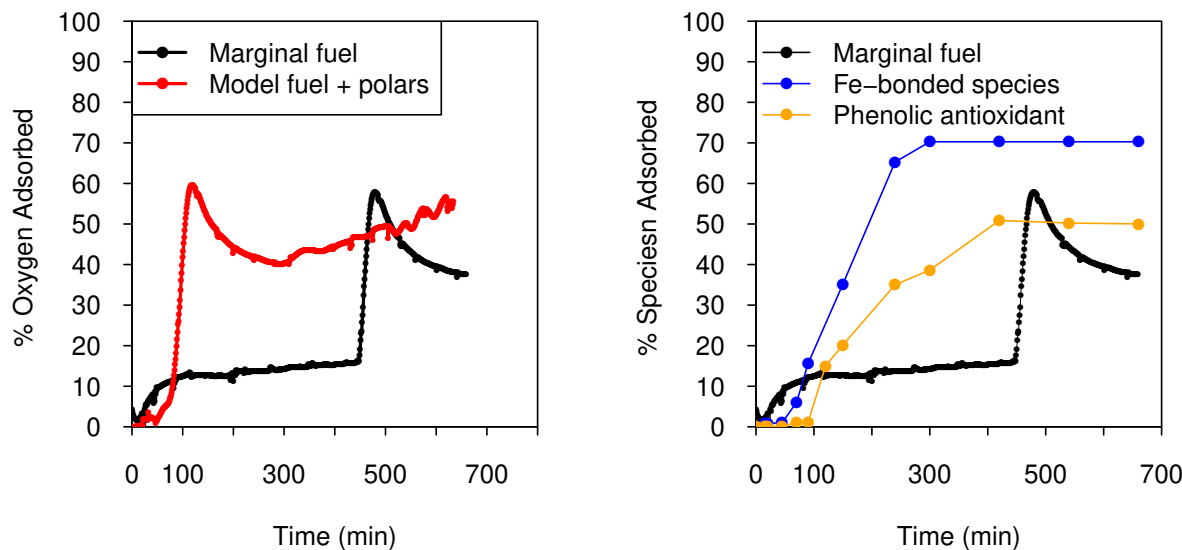
(a) O_2 adsorption from marginal and model fuel

(b) Adsorption of phenolic antioxidants and Fe-bonded species from marginal fuel

Figure 7: a) Comparison of multi stage O_2 adsorption from marginal and model fuel, b) Fe-bonded and phenolic antioxidant adsorption from marginal fuelthe samples for polar separation were taken through a valve, 2 m downstream of the packed bed

508 Role of hydroperoxides in near-complete fuel deoxygenated condition

509 Given the results of Fe-bonded and phenolic adsorption by zeolite 3.7Å and combining these

510 to the relatively high concentration of hydroperoxides in the marginal fuel as shown in ta-

511 ble2, we proposed an additional chemical pathway to the BAS, known as self-reaction of

512 hydroperoxides. We used quantum chemistry to determine the kinetic parameters of this

513 chemical pathway to interpret the results shown in figure3a and figure3b.

514

515 The self-reaction of hydroperoxides was first proposed by Bateman[54] and cited by Denisov,[7]

516 as presented schematically in rxn7.

$$2\,\mathrm{ROOH} \longrightarrow \mathrm{RO}\cdot + \mathrm{H_2O} + \mathrm{RO_2}\cdot \tag{7}$$

As presented in figure 8, quantum chemistry calculations indicate that the self-reaction of hydroperoxides can proceed through a concerted and two-step route. These pathways are thermodynamically favourable and the radicals, formed during the first step of a two-step pathway, react with no barrier to form polar and non-radical products. Interestingly, one of which is another hydroperoxide species, therefore maintaining autoxidation cycle through their role in the propagation stage. We also noted that the transition state between the peroxyl and alkoxy radical fragments and the final products could not be located. This indicates that the self-reaction of hydroperoxides is barrierless or the energy barrier is very small. As such, the overall barrier to reaction is likely to stand as $+33.6$ kcal mol^{-1}.

A number of conclusions can be drawn from these calculations: the first conclusion is that an energy difference of $+4.2$ kcal mol^{-1}, between the two possible pathways, indicates that the reaction proceeds through the two step mechanism. The second conclusion that can be made from these calculations is that, even with a barrier of $+33.6$ kcal mol^{-1}, this pathway is a viable reaction in the thermally-stressed fuel, as it is approximately 10 kcal mol^{-1} lower than that for the thermal decomposition of hydroperoxides, with the same order for the pre-exponential factor of around $1\mathrm{x}10^{15}(\mathrm{mol,L,s})$.[18,19,55]

It is important to note that the DFT calculations represent the upper value of the reaction barrier; however, due to the poor treatment of the electronic structure in this system, the barrier is likely over-estimated. This is also supported by the values presented in the literature[7,54], although the exact methods used to determine those barriers are unknown. As

540 such, future work will be carried out using high level quantum chemistry theories to better

541 understand this reaction.

542

543 In summary, given that the overriding difference between the two baseline fuels tested in this

544 work was the concentration of hydroperoxides and considering the fact that the self-reaction

545 of hydroperoxides is kinetically more probable than thermal decomposition, it is likely that

546 the self-reaction of hydroperoxide is responsible for the increasing deposition tendency of the

547 treated marginal fuel over the thermal exposure time in the HiReTS tube. It is important to

548 note that the underlying chemistry of hydroperoxides and thier link to the surface deposition

549 requires further research.

550

551

552 In the case of near-complete deoxygenation of marginal fuel, as illustrated in figure3a, the

553 high propensity of fuel for deposit formation, is likely to be attributed to the catalytic decom-

554 position of hydroperoxides, as this class of reactions requires approximately $+10$ kcal mol^{-1}.[18]

555 This class of reactions is responsible for the formation of a series of chemical species, known

556 as the secondary products of autoxidation. These include: alcohols, ketones, aldehydes and

557 acids which collectively contribute to the formation of surface deposition through complex

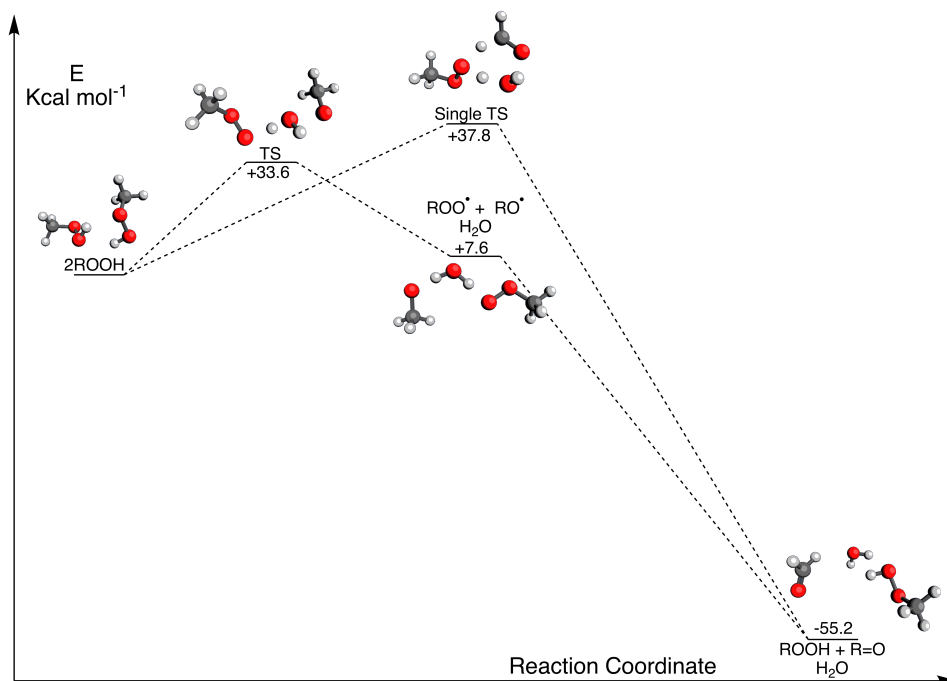558 reactions with reactive sulfures, antioxidants and polar nitrogen.

Figure 8: Calculated reaction surface of the self reaction of methyl peroxide. The calculations were performed at the UB3LYP/cc-pVTZ/PCM (heptane) level of theory. It is clear that the reaction proceeds through a two step mechanism, at the energy barrier difference of +4.2kcal mol^{-1} means +99% of the reaction goes through this pathway at expected temperatures.

Calculation of competitive adsorption in packed bed reactor

Simulation of simultaneous adsorption of various groups of polars and dissolved O_2 by the packed bed is interesting from the microscopic modelling point of view. However, as mentioned in the modelling section of this article, a number of assumptions and theories should be integrated into the microscopic modelling approach which collectively makes the simulation rather challenging and computationally expensive. These include the individual molecular motion, the physico-chemical interactions between zeolite pores and adsorbing molecules(polar species and molecular O_2), as well as the interactions amongst molecules during diffusion and adsorption. Understanding these interactions require an extensive quantum chemistry and molecular dynamics calculations along with experiments which is beyond the scope of this article. Therefore, for simplicity, in our macroscopic modelling approach,

570 all the molecular-level assumptions were ignored.

571

572 Initially, it was assumed that the dissolved oxygen separation in the packed bed reactor is

573 purely based on the physisorption. For the physisorption, the only tuning parameters are

574 the last two in table4, namely "Freundlich constant for oxygen" and "Freundlich exponent for

575 oxygen ". These parameters can control the adsorption capacity and the induction period

576 prior to the first phase of adsorption. For simplicity, to include the interference of chemical

577 interactions during physisorption, all possible chemical interactions were treated as one phe-

578 nomenological metamathematical expression, purely based on the experimental observations

579 presented in figure 7, using the reaction source term in equation2.

580

581 The modelling results presented in the figure9a illustrate the adsorption of dissolved O_2 onto

582 the bed of zeolite 3.7Å. The modelling results are in good agreement with the partial ad-

583 sorption of dissolved O_2 from marginal fuel during the induction period and the first and

584 second phases of adsorption. However, there is a discrepancy between the model results and

585 the measurement data after the second phase of adsorption.

586

587 A closer look at the modelling results indicates that the beginning of adsorption process

588 was predicted with a good degree of accuracy as shown in the figure9b. The beginning of

589 adsorption process is manifested by an induction period which is likely to be attributed to

590 the adsorption of the oxygenated species as observed in figure6b. This demonstrates that

591 the model can be used for calculation of time needed for the beginning of adsorption of the

592 oxygenated species. As the results of figure9b show, after $t = 50\ min$, the model results

593 indicate a plateau while the measurements show a slow adsorption of dissolved O_2. However,

594 this requires more in-depth understanding of physico-chemical interactions during this phase.

595
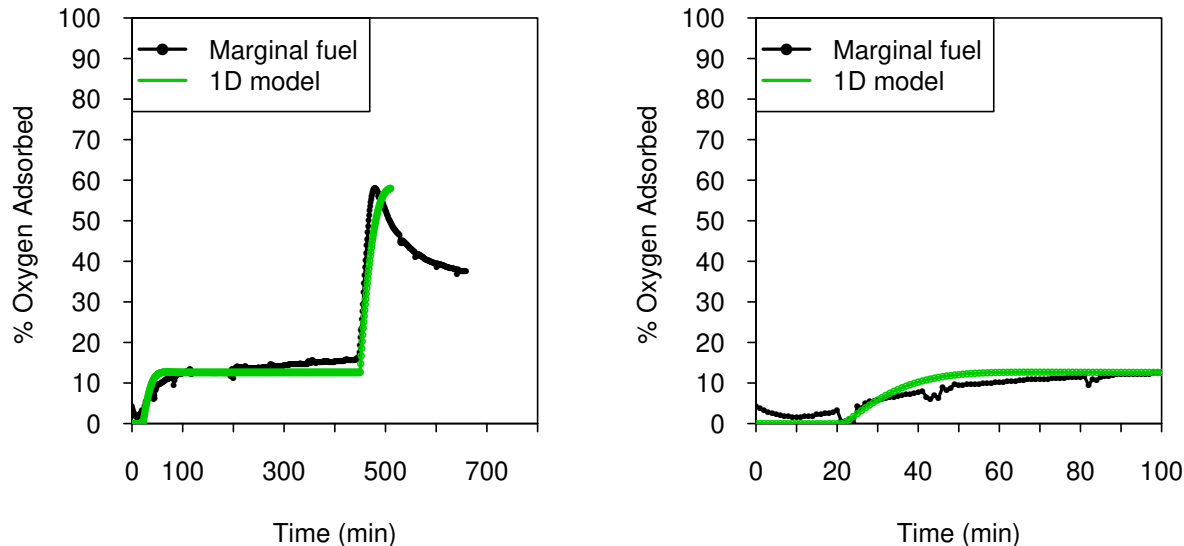
(a) Calculation of different stages of adsorption

(b) Calculation of induction period and first stage of adsorption

Figure 9: Prediction of different stages of O_2 during competitive adsorption from marginal through the packed bed

Conclusions

The sensitivity of deposition propensity of a fuel, with marginal thermal oxidative stability, to deoxygenation and polar species removal was studied. The deoxygenation was achieved by N_2 purging while polar species removal was carried out by the application of two types of bespoke adsorbents including zeolite 3.7Å and 4.5Å in a packed bed reactor.

Our experimental findings demonstrate that when the concentration of total hydroperoxides in jet fuel is relatively high, the fuel deoxygenation is not an effective way to reduce deposition propensity. This is likely to be attributed to the the self-reaction of hydroperoxides which results in generation of primary and secondary oxygenated products(hydroperoxides and spices with carbonyl groups) thus participating in prorogation stage of fuel autoxidation. Our quantum chemistry calculations indicate that self-reaction of hydroperoxides is a

608 thermodynamically viable two-step reaction.

609

610 The competitive adsorption of O_2 with some of the polar species by zeolite 3.7Å for a model

611 fuel was studied. It was found that the beginning of O_2 adsorption is hindered by the fast

612 adsorption of the oxygenated species. Moreover, when the oxygenated species reached a

613 plateau, O_2 adsorption proceeded with fast kinetics. A maximum uptake capacity of ap-

614 proximately 60% was recorded for O_2 followed by a moderate decrease. It appears that

615 the reduction in O_2 adsorption corresponds to the fast adsorption of aniline, and moderate

616 adsorption of BHT and Fe naphthenate. Furthermore, the results showed that when the

617 adsorption of these species reaches a plateau, O_2 begins to adsorb again with slower kinetics.

618

619 The similar trend for competitive O_2 adsorption by zeolite 3.7Å for marginal fuel was ob-

620 served. However, it can be seen that the beginning of O_2 adsorption time is substantially

621 longer than that in the model fuel doped with the polar species. This is likely to be at-

622 tributed to the lower concentration of polar species in the marginal fuel in comparison with

623 the model fuel. There is a similar trend for decrease of O_2 adsorption for marginal fuel after

624 the maximum uptake capacity which resembles the competitive adsorption of Fe- bonded

625 molecules and phenolic antioxidant.

626

627 The results of one dimensional model can be used to calculate the duration of hindrance for

628 O_2 adsorption and the maximum uptake capacity of O_2. The time needed for the start of

629 O_2adsorption can be used as an indication for the adsorption of oxygenated products. The

630 model falls short of being applicable to calculate the second phase of competitive adsorption.

631 Fundamental physical model is required to build an integrated model to predict the entire

632 process.

633

Acknowledgement

References

(1) Hazlett, R N, *Thermal Oxidation Stability of Aviation Turbine Fuels*; ASTM, 1991.

(2) Beaver, B.; Gao, L.; Burgess-Clifford, C.; Sobkowiak, M. On the Mechanisms of Formation of Thermal Oxidative Deposits in Jet Fuels. Are Unified Mechanisms Possible for Both Storage and Thermal Oxidative Deposit Formation for Middle Distillate Fuels? *Energy & Fuels* **2005**, *19*, 1574–1579.

(3) Reddy, K. T.; Cernansky, N. P.; Cohen, R. S. Modified reaction mechanism of aerated n-dodecane liquid flowing over heated metal tubes. *Energy & Fuels* **1988**, *2*, 205–213.

(4) Jones, E. G.; Balster, W. J. Phenomenological Study of the Formation of Insolubles in a Jet-A Fuel. *Energy & Fuels* **1993**, *7*, 968–977.

(5) Jones, E. G.; Balster, L. M.; Balster, W. J. Autoxidation of Aviation Fuels in Heated Tubes : Surface Effects. *Energy & Fuels* **1996**, *10*, 831–836.

(6) Kuprowicz, N. J.; Ervin, J. S.; Zabarnick, S. Modeling the liquid-phase oxidation of hydrocarbons over a range of temperatures and dissolved oxygen concentrations with pseudo-detailed chemical kinetics. *Fuel* **2004**, *83*, 1795–1801.

(7) Denisov, E. T.; Afanas'ev, I. B. *Oxidation and Antioxidants in Organic Chemistry and Biology*; CRC Press, 2005.

(8) Jones, E. G.; Balster, L. M. Impact of Additives on the Autoxidation of a Thermally Stable Aviation Fuel. *Energy & Fuels* **1997**, *11*, 610–614.

(9) Grinstead, B.; Zabarnick, S. Studies of Jet Fuel Thermal Stability, Oxidation, and Additives Using an Isothermal Oxidation Apparatus Equipped with an Oxygen Sensor. *Energy & Fuels* **1999**, *13*, 756–760.

(10) Taylor, W. F. Deposit Formation from Deoxygenated Hydrocarbons. II. Effect of Trace Sulfur Compounds. *Industrial & Engineering Chemistry Product Research and Development* **1976**, *15*, 64–68.

(11) Zabarnick, S.; Mick, M. S. Inhibition of Jet Fuel Oxidation by Addition of Hydroperoxide-Decomposing Species. *Industrial & Engineering Chemistry Research* **1999**, 3557–3563.

(12) Taylor, W. F.; Frankenfeld, J. W. Deposit Formation from Deoxygenated Hydrocarbons. 3. Effects of Trace Nitrogen and Oxygen Compounds. *Industrial & Engineering Chemistry Product Research and Development* **1978**, *17*, 86–90.

(13) Ervin, J. S.; Williams, T. F. Dissolved Oxygen Concentration and Jet Fuel Deposition. *Industrial & Engineering Chemistry Research* **1996**, *35*, 899–904.

(14) Balster, L. M.; Zabarnick, S.; Striebich, R. C.; Shafer, L. M.; West, Z. J. Analysis of Polar Species in Jet Fuel and Determination of Their Role in Autoxidative Deposit Formation. *Energy & Fuels* **2006**, *20*, 2564–2571.

(15) Striebich, R. C.; Contreras, J.; Balster, L. M.; West, Z.; Shafer, L. M.; Zabarnick, S. Identification of Polar Species in Aviation Fuels using Multidimensional Gas Chromatography-Time of Flight Mass Spectrometry. *Energy & Fuels* **2009**, *23*, 5474–5482.

(16) Commodo, M.; Fabris, I.; Groth, C. P. T.; Gülder, Ö. L. Analysis of Aviation Fuel Thermal Oxidative Stability by Electrospray Ionization Mass Spectrometry (ESI–MS). *Energy & Fuels* **2011**, *25*, 2142–2150.

(17) Taylor W F, *Development of High Stability Fuel, ESSO Research and Engineering Report*; 1972.

(18) Kuprowicz, N. J.; Zabarnick, S.; West, Z. J.; Ervin, J. S.; Edwards, T. Use of Measured Species Class Concentrations With Chemical Kinetic Modelling for the Prediction of Autoxidation and Deposition of Jet Fuels. *Energy & Fuels* **2007**, *21*, 530–544.

(19) Zabarnick, S. Chemical Kinetic Modeling of Jet Fuel Autoxidation and Antioxidant Chemistry. *Industrial & Engineering Chemistry Research* **1993**, *32*, 1012–1017.

(20) West, Z. J.; Zabarnick, S.; Striebich, R. C. Determination of Hydroperoxides in Jet Fuel via Reaction with Triphenylphosphine. *Industrial & Engineering Chemistry Research* **2005**, *44*, 3377–3383.

(21) Pickard, J. M.; Jones, E. G. Catalysis of Jet-A Fuel Autoxidation by Fe_2O_3. *Energy & Fuels* **1997**, *11*, 1232–1236.

(22) Zabarnick, S.; DeWitt, M. J.; Striebich, R. C.; Gunasekera, T. S.; Ervin, J.; Briones, A.; Shafer, L.; Fernando, S.; Graham, J.; West, Z.; Stouffer, S.; Vangsness, M.; Harruff-Miller, B. *Fuels and Combustion Technologies for Aerospace Propulsion*; 2016.

(23) Spadaccini, L.; Huang, H. On-Line Fuel Deoxygenation for Coke Suppression. *Journal of Engineering for Gas Turbines and Power* **2003**, *125*, 686–692.

(24) Taylor, W. F. Deposit Formation from Deoxygenated Hydrocarbons. I. General Features. *Industrial & Engineering Chemistry Product Research and Development* **1974**, *13*, 133–138.

(25) Frankenfeld, J. W.; Taylor, W. F. Deposit Formation from Deoxygenated Hydrocarbons. 4. Studies in Pure Compound Systems. *Industrial & Engineering Chemistry Product Research and Development* **1980**, *19*, 65–70.

(26) Naegeli, D, The Role of Sulfur in the Thermal Stability of Jet Fuel. ASME-GT. 1999.

(27) *Handbook of Aviation Fuel Properties*, 4th ed.; Coordinating Research Council, 2014.

(28) Darrah S, *Jet Fuel Deoxygenation, AFWAL-TR-88-2081 Interim Report,*; 1988.

(29) Van Bekkum, H.; Flanigen, E. M.; Jensen, J. C. *Introduction to Zeolite and Science Practice* ; Elsevier, 1991.

(30) Kulprathipanja, S. *Zeolites in Industrial Separation and Catalysis* ; Willey, 2010.

(31) Bendoraitis, J. G.; Chester, A. W.; Dwyer, F. G.; Garwood, W. E. Pore Size and Shape Effects in Zeolite Catalysis. *Studies in Surface Science and Catalysis* **1986**, *28*, 669–675.

(32) Mallon, E. E.; Bhan, A.; Tsapatsis, M. Driving Forces for Adsorption of Polyols onto Zeolites from Aqueous Solutions. *The Journal of Physical Chemistry B* **2010**, *114*, 1939–1945, PMID: 20070098.

(33) Nguyen, C. M.; Reyniers, M. F.; Marin, B. G. Theoretical study of the adsorption of C1-C4 primary alcohols in HZSM5. *Physical Chemistry Chemical Physics* **2010**, *12*, 9481–9493.

(34) Jha, B. and Singh, D N, *Basics of Zeolites. In: Fly Ash Zeolites. Advanced Structured Materials*; Elsevier Inc., 2016.

(35) Density functional theory study on the adsorption of H 2S and other claus process tail gas components on copper- and silver-exchanged Y zeolites. *Journal of Physical Chemistry C* **2012**, *116*, 3561–3575.

(36) Smith, D. G. A.; Patkowski, K. Benchmarking the CO2 Adsorption Energy on Carbon Nanotubes. *The Journal of Physical Chemistry C* **2015**, *119*, 4934–4948.

(37) Shang, J.; Li, G.; Webley, P. A.; Liu, J. Z. A density functional theory study for the adsorption of various gases on a caesium-exchanged trapdoor chabazite. *Computational Materials Science* **2016**, *122*, 307–313.

(38) Fischer, M.; Bell, R. G. Modeling CO2 Adsorption in Zeolites Using DFT-Derived Charges: Comparing System-Specific and Generic Models. *The Journal of Physical Chemistry C* **2013**, *117*, 24446–24454.

(39) Alborzi, E.; Blakey, S.; Ghadbeigi, H.; Pinna, C.; Lewis, C. Investigation of surface deposition in a simulated fuel injector feed arm with sudden expansion/contraction. *Fuel* **2016**, *186*, 534 – 543.

(40) Alborzi, E.; Blakey, S.; Ghadbeigi, H.; Pinna, C. Prediction of growth of jet fuel autoxidative deposits at inner surface of a replicated jet engine burner feed arm. *Fuel* **2018**, *214*, 528–537.

(41) Kärger, J. Measurement of Diffusion in Zeolites—A Never Ending Challenge? *Adsorption* **2003**, *9*, 29–35.

(42) Becke, A. D. Density-functional thermochemistry. III. The role of exact exchange. *The Journal of Chemical Physics* **1993**, *98*, 5648–5652.

(43) Dunning, T. H. Gaussian basis sets for use in correlated molecular calculations. I. The atoms boron through neon and hydrogen. *The Journal of Chemical Physics* **1989**, *90*, 1007–1023.

(44) Wilson, A. K.; van Mourik, T.; Dunning, T. H. Gaussian basis sets for use in correlated molecular calculations. VI. Sextuple zeta correlation consistent basis sets for boron through neon. *Journal of Molecular Structure: THEOCHEM* **1996**, *388*, 339–349.

748 (45) Kendall, R. A.; Dunning, T. H.; Harrison, R. J. Electron affinities of the first-row atoms

749 revisited. Systematic basis sets and wave functions. *The Journal of Chemical Physics*

750 **1992**, *96*, 6796–6806.

751 (46) Woon, D. E.; Dunning, T. H. Gaussian basis sets for use in correlated molecular cal-

752 culations. III. The atoms aluminum through argon. *The Journal of Chemical Physics*

753 **1993**, *98*, 1358–1371.

754 (47) Peterson, K. A.; Woon, D. E.; Dunning, T. H. Benchmark calculations with correlated

755 molecular wave functions. IV. The classical barrier height of the H+H2=H2+H reaction.

756 *The Journal of Chemical Physics* **1994**, *100*, 7410–7415.

757 (48) Tomasi, J.; Mennucci, B.; Cammi, R. Quantum mechanical continuum solvation models.

758 *Chemical Reviews* **2005**, *105*, 2999–3093.

759 (49) Ochterski, J. W.; Ph, D. Thermochemistry in Gaussian. *Gaussian Inc Pittsburgh PA*

760 **2000**, *264*, 1–19.

761 (50) M, H. C. *Hansen Solubility Parameters, A User's Handbook*, 2nd ed.; CRC Press, 2007.

762 (51) Abbot, S. HSP Basics. `https://www.stevenabbott.co.uk/practical-solubility/`

763 `hsp-basics.php`.

764 (52) Javadian, S.; Ektefa, F. An efficient approach to explore the adsorption of benzene

765 and phenol on nanostructured catalysts: a DFT analysis. *RSC Adv.* **2015**, *5*, 100799–

766 100808.

767 (53) Stefanis, E.; Panayiotou, C. Prediction of Hansen Solubility Parameters with a New

768 Group-Contribution Method. *International Journal of Thermophysics* **2008**, *29*, 568–

769 585.

770 (54) Bateman, L.; Hughes, H.; Morris, A. Hydroperoxide decomposition in relation to the

771 initiation of radical chain reactions. *Discuss. Faraday Soc.* **1953**, *14*, 190–199.

772 (55) Zabarnick, S. Pseudo-Detailed Chemical Kinetic Modeling of Antioxidant Chemistry

773 for Jet Fuel Applications. *Energy & Fuels* **1998**, *0624*, 547–553.